Electronic Supplementary Material (ESI) for Physical Chemistry Chemical Physics.

Supplementary Information

Direct Time-Resolved Detection and Quantification of Key Reactive Intermediates in Diethyl Ether Oxidation at T = 450 – 600 K.

Maria Demireva*, Kendrew Au, and Leonid Sheps*

Combustion Research Facility, Sandia National Laboratories, Livermore, California 94551, United States

*Corresponding authors: lsheps@sandia.gov, mdemire@sandia.gov.

Experimental conditions of the present diethyl ether (DEE) low-temperature oxidation study.

Table S1. Summary of experimental conditions used in the present study. Bold font indicates the baseline conditions at which absolute PI cross-sections of ROO•, •OOQOOH, and KHP were determined.

T (K)	P (Torr)	Photon Energy (eV)	DEE (cm^{-3})	O_2 (cm^{-3})	OxCl (cm^{-3})	$Cl_{t=0}$ (cm^{-3})[a]
450	**7500**	**8.5 – 11**	**1×10^{14}**	**7×10^{17}**	**3×10^{15}**	**3.5×10^{12}**
500	7500	8.5 – 11	1×10^{14}	7×10^{17}	3×10^{15}	5×10^{12}
550	7500	8.5 – 11	1×10^{14}	7×10^{17}	3×10^{15}	3.5×10^{12}
600	7500	8.5 – 11	1×10^{14}	7×10^{17}	3×10^{15}	3.5×10^{12}
500	1500	8.5 – 11	1×10^{14}	7×10^{17}	3×10^{15}	5×10^{12}
500	3750	8.5 – 11	1×10^{14}	7×10^{17}	3×10^{15}	5×10^{12}
500	7300	8.7 – 11	1×10^{14}	0	3×10^{15}	3×10^{12}
500	7300	8.7 – 11	1×10^{14}	1.7×10^{17}	3×10^{15}	3×10^{12}
500	7300	8.7 – 11	1×10^{14}	7×10^{17}	3×10^{15}	3×10^{12}
500	7300	8.7 – 11	1×10^{14}	3.5×10^{18}	3×10^{15}	3×10^{12}
500	7300	8.7 – 11	1×10^{14}	7×10^{18}	3×10^{15}	3×10^{12}
500	7300	9.0 – 10.8	2×10^{15}	8×10^{18}	1×10^{16}	2×10^{14}
400	7300	8.7 – 11	1×10^{14}	1.7×10^{17}	3×10^{15}	4×10^{12}
400	7300	8.7 – 11	1×10^{14}	7×10^{17}	3×10^{15}	4×10^{12}
400	7300	8.7 – 11	1×10^{14}	3.5×10^{18}	3×10^{15}	4×10^{12}
400	7300	8.7 – 11	1×10^{14}	7×10^{18}	3×10^{15}	4×10^{12}
450	50[b]	8.5 – 11	1×10^{14}	2.5×10^{17}	8×10^{13}	5×10^{12}

[a] Estimated concentration.
[b] Acquired on low-pressure MPIMS instrument.

Measurement of absolute photoionization (PI) cross-sections.

All reference PI spectra were measured in a low-pressure MPIMS instrument,[1] using gas mixtures of the target compound and propene, diluted in He. These spectra were acquired as a function of VUV photon energy and absolute PI cross-sections were determined from equation (1), using propene as a reference with known PI cross-section.[2] Unless noted otherwise, the estimated uncertainty in the cross-sections is ±20% due to the ±20% uncertainty in the PI cross-section of the reference compound, propene.

Ethyl Vinyl Ether. We used a mixture of 1.5% ethyl vinyl ether/1.7% propene in He at P = 4 Torr and T = 600 K. The results are provided in Figure S1 and Table S2.

Diethyl Ether. We used a mixture of 2.4% DEE/2.0% propene in He at P = 4 Torr and T = 600 K. The PI cross-sections, presented in Figure S2 and Table S3, are in fair agreement with previous results.[3]

Acetaldehyde. We used a mixture of 1.2% CH_3CHO/1.0% propene in He at P = 4 Torr and T = 300 K. The results in Figure S3 and Table S4 are in good agreement with previous work.[4]

***Acetic Anhydride*.** We used a mixture of 1.5% acetic anhydride/0.1% propene in He at T = 500 K and P = 10 Torr and 50 Torr. During the measurement we noticed a small signal due to acetic acid. In addition, the PI cross-section derived from the 10 Torr data was slightly different from that at 50 Torr, as shown in Figure S4. We suspect that these observations indicate that some acetic anhydride was hydrolyzed before or in the reactor, rendering its concentration uncertain. Therefore, we do not report absolute PI cross-sections of acetic anhydride and treat these data as estimates only with uncertainty of at least 50%. Qualitatively, photoionization of acetic anhydride at energies up to 11 eV is dominated by the DI peak at *m/z* 43. The parent cation at *m/z* 102 is ~300 times less intense and a second DI peak at *m/z* 87 is ~40 times less intense.

2-Methyl-1,3-Dioxolane. We used a mixture of 2.5% 2-methyl-1,3-dioxolane/8.5% propene in He at P = 4 Torr and T = 600 K. The results are presented in Figure S5 and Table S5.

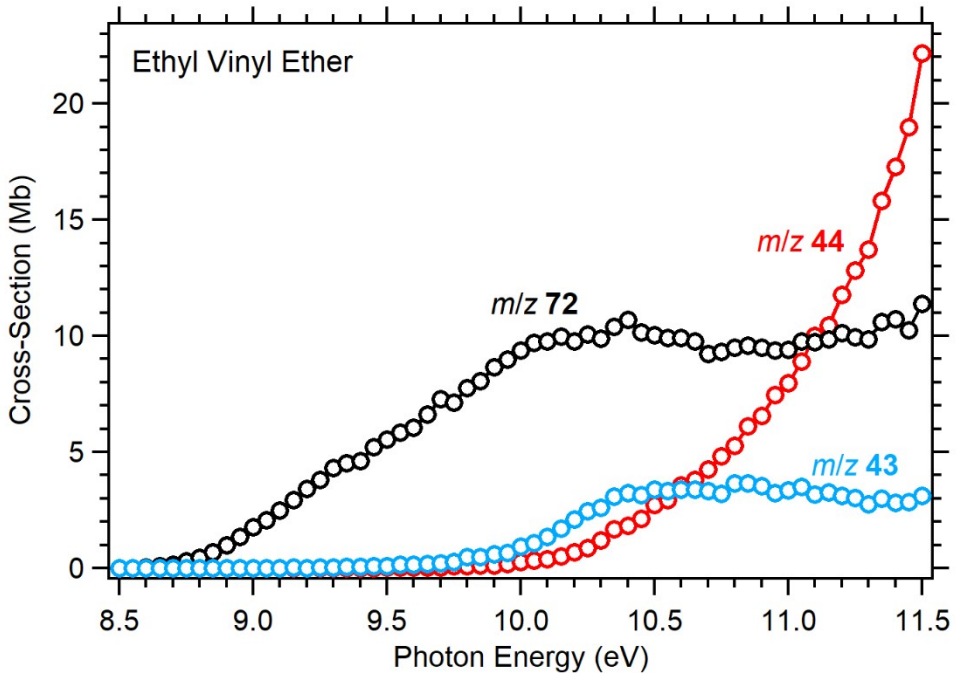

Figure S1. Absolute PI cross-section for the parent cation of ethyl vinyl ether at *m/z* 72 and for DI fragments at *m/z* 44 and 43.

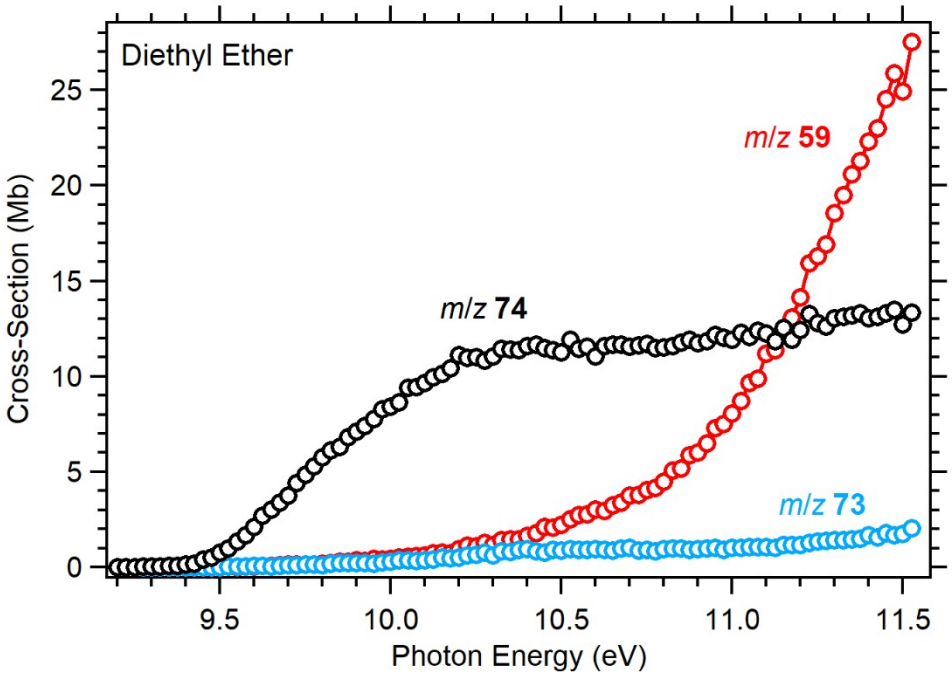

Figure S2. Absolute PI cross-section for the parent cation of diethyl ether at *m*/*z* 74 and for DI fragments at *m*/*z* 73 and 59.

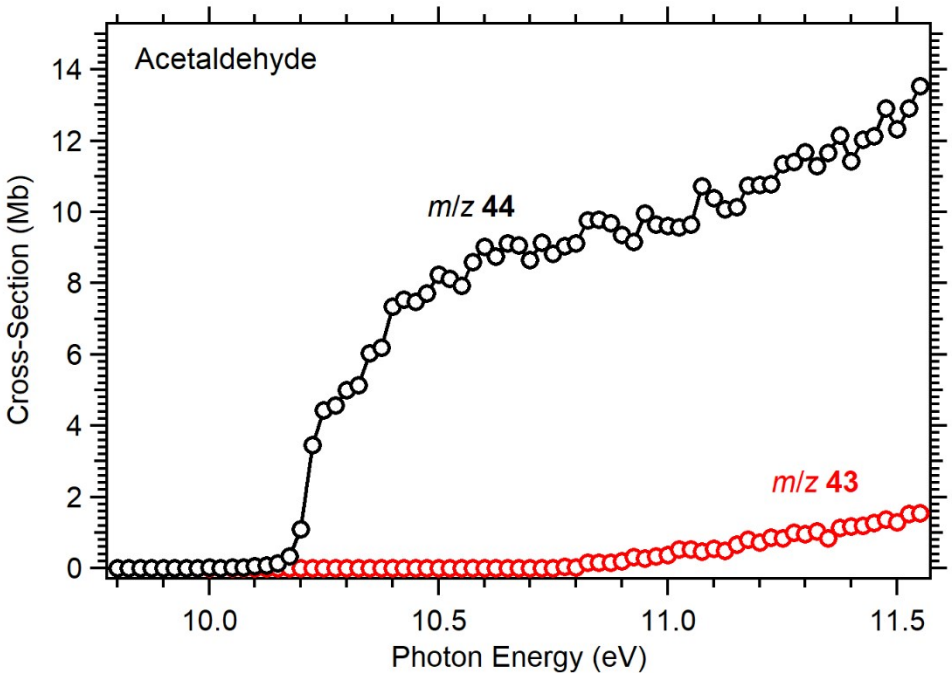

Figure S3. Absolute PI cross-section for the parent cation of acetaldehyde at *m*/*z* 44 and for DI fragment at *m*/*z* 43.

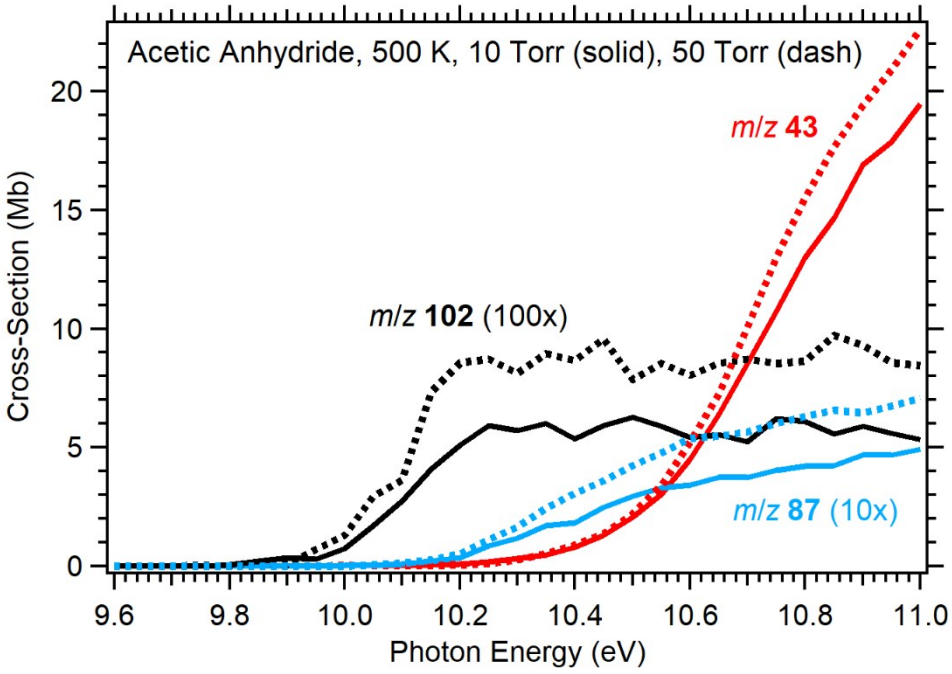

Figure S4. Estimated PI cross-section for the parent cation of acetic anhydride at *m*/*z* 102 and for DI fragments at *m*/*z* 87 and 43.

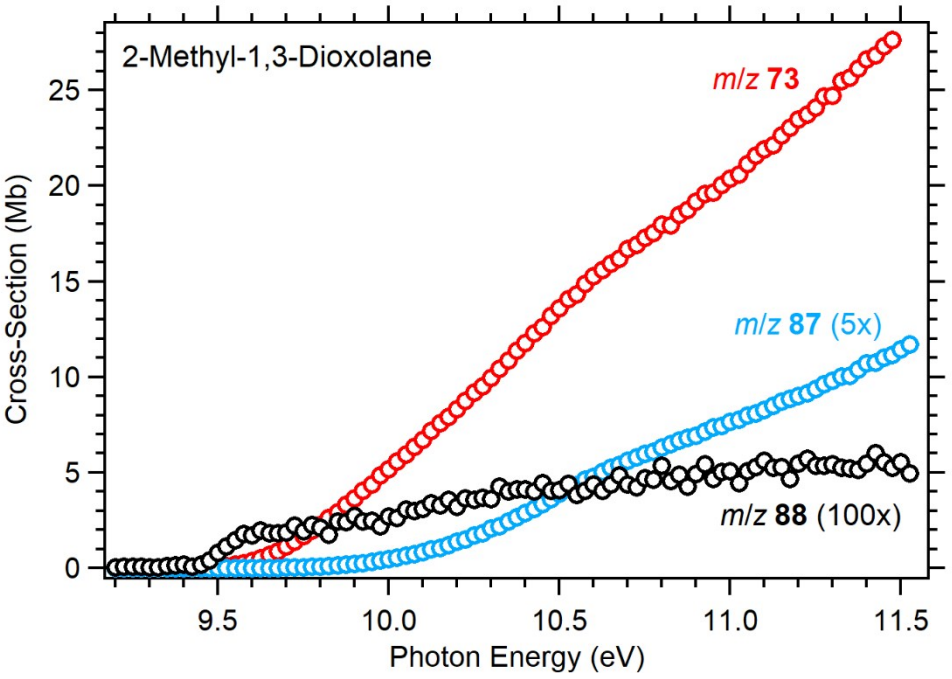

Figure S5. Absolute PI cross-section for the parent cation of 2-methyl-1,3-dioxolane at *m*/*z* 88 and for DI fragments at *m*/*z* 87 and 73.

Table S2. Absolute PI cross-sections (in Mb) for ethyl vinyl ether.

Energy (eV)	*m/z* 72	*m/z* 44	*m/z* 43	Energy (eV)	*m/z* 72	*m/z* 44	*m/z* 43
8.50	0.00	0.00	0.00	10.05	9.71	0.32	1.08
8.55	0.01	0.00	0.00	10.10	9.75	0.39	1.34
8.60	0.04	0.00	0.00	10.15	9.97	0.51	1.72
8.65	0.10	0.01	0.00	10.20	9.75	0.70	2.09
8.70	0.14	0.00	0.00	10.25	10.06	0.85	2.47
8.75	0.29	0.00	0.00	10.30	9.87	1.20	2.61
8.80	0.46	0.00	0.00	10.35	10.38	1.69	3.07
8.85	0.68	0.00	0.00	10.40	10.68	1.82	3.23
8.90	1.00	0.00	0.01	10.45	10.14	2.13	3.15
8.95	1.36	0.01	0.00	10.50	10.03	2.73	3.39
9.00	1.75	0.00	0.01	10.55	9.91	2.93	3.32
9.05	2.07	0.01	0.00	10.60	9.90	3.56	3.37
9.10	2.49	0.01	0.00	10.65	9.76	3.80	3.38
9.15	2.94	0.00	0.03	10.70	9.22	4.27	3.32
9.20	3.41	0.01	0.01	10.75	9.30	4.83	3.20
9.25	3.80	0.00	0.02	10.80	9.50	5.27	3.65
9.30	4.32	0.01	0.04	10.85	9.57	6.12	3.65
9.35	4.53	0.00	0.07	10.90	9.51	6.57	3.54
9.40	4.63	0.00	0.06	10.95	9.39	7.46	3.24
9.45	5.21	0.01	0.09	11.00	9.41	7.97	3.36
9.50	5.55	0.04	0.08	11.05	9.77	8.89	3.51
9.55	5.84	0.03	0.14	11.10	9.74	10.00	3.17
9.60	6.04	0.03	0.14	11.15	9.85	10.46	3.26
9.65	6.60	0.04	0.18	11.20	10.12	11.78	3.10
9.70	7.27	0.03	0.22	11.25	9.95	12.81	3.03
9.75	7.14	0.08	0.28	11.30	9.86	13.71	2.75
9.80	7.76	0.09	0.48	11.35	10.60	15.81	2.99
9.85	8.05	0.11	0.47	11.40	10.72	17.28	2.81
9.90	8.65	0.13	0.59	11.45	10.24	19.00	2.84
9.95	8.97	0.16	0.67	11.50	11.37	22.16	3.11
10.00	9.36	0.28	0.93				

Table S3. Absolute PI cross-sections (in Mb) for diethyl ether.

Energy (eV)	*m/z* 74	*m/z* 73	*m/z* 59	Energy (eV)	*m/z* 74	*m/z* 73	*m/z* 59
9.200	0.00	0.00	0.00	10.375	11.39	0.93	1.45
9.225	0.01	0.00	0.00	10.400	11.58	0.93	1.65
9.250	0.01	0.00	0.00	10.425	11.67	0.83	1.79
9.275	0.02	0.00	0.00	10.450	11.47	0.77	2.12
9.300	0.03	0.00	0.00	10.475	11.36	0.91	2.08
9.325	0.05	0.00	0.01	10.500	11.26	0.88	2.22
9.350	0.07	0.00	0.00	10.525	11.92	0.93	2.53
9.375	0.09	0.00	0.00	10.550	11.46	0.93	2.73
9.400	0.15	0.00	0.00	10.575	11.57	0.91	2.78
9.425	0.19	0.01	0.01	10.600	11.06	0.96	3.03
9.450	0.39	0.00	0.01	10.625	11.59	0.90	2.95
9.475	0.52	0.01	0.01	10.650	11.68	0.86	3.25
9.500	0.76	0.01	0.02	10.675	11.66	0.97	3.39
9.525	0.98	0.02	0.03	10.700	11.56	1.03	3.75
9.550	1.36	0.02	0.01	10.725	11.64	0.86	3.80
9.575	1.68	0.03	0.03	10.750	11.69	0.92	4.04
9.600	2.12	0.06	0.05	10.775	11.47	0.85	4.14
9.625	2.70	0.06	0.07	10.800	11.53	0.94	4.50
9.650	3.03	0.05	0.07	10.825	11.59	0.99	5.08
9.675	3.37	0.06	0.12	10.850	11.79	1.00	5.17
9.700	3.76	0.10	0.15	10.875	11.91	0.91	5.87
9.725	4.40	0.10	0.13	10.900	11.76	0.94	6.00
9.750	4.85	0.14	0.14	10.925	11.85	0.98	6.51

9.775	5.28	0.13	0.15	10.950	12.19	1.01	7.30
9.800	5.77	0.12	0.17	10.975	12.02	0.92	7.50
9.825	6.14	0.20	0.24	11.000	11.94	1.01	8.07
9.850	6.29	0.21	0.30	11.025	12.29	1.02	8.70
9.875	6.81	0.21	0.29	11.050	12.07	1.06	9.65
9.900	7.12	0.21	0.35	11.075	12.40	1.06	9.89
9.925	7.40	0.20	0.33	11.100	12.23	1.04	11.19
9.950	7.76	0.20	0.43	11.125	11.86	1.03	11.39
9.975	8.28	0.26	0.38	11.150	12.53	1.16	12.32
10.000	8.43	0.29	0.44	11.175	11.93	1.18	13.08
10.025	8.65	0.37	0.51	11.200	12.45	1.18	14.13
10.050	9.40	0.38	0.56	11.225	13.29	1.29	15.92
10.075	9.45	0.34	0.58	11.250	12.81	1.33	16.30
10.100	9.65	0.38	0.64	11.275	12.63	1.40	16.90
10.125	9.97	0.41	0.71	11.300	13.06	1.43	18.56
10.150	10.14	0.52	0.75	11.325	13.12	1.40	19.51
10.175	10.42	0.47	0.74	11.350	13.19	1.46	20.58
10.200	11.12	0.51	0.95	11.375	13.30	1.48	21.31
10.225	10.98	0.61	1.12	11.400	13.04	1.67	22.32
10.250	11.03	0.66	1.11	11.425	13.12	1.59	22.99
10.275	10.84	0.77	1.27	11.450	13.31	1.79	24.52
10.300	11.03	0.64	1.18	11.475	13.48	1.68	25.89
10.325	11.45	0.83	1.41	11.500	12.71	1.73	24.94
10.350	11.40	0.79	1.44	11.525	13.34	2.03	27.52

Table S4. Absolute PI cross-sections (in Mb) for acetaldehyde.

Energy (eV)	*m*/*z* 44	*m*/*z* 43	Energy (eV)	*m*/*z* 44	*m*/*z* 43
9.900	0.00	0.00	10.825	9.77	0.16
9.925	0.00	0.00	10.850	9.78	0.15
9.950	0.00	0.00	10.875	9.69	0.16
9.975	0.01	0.00	10.900	9.35	0.20
10.000	0.01	0.00	10.925	9.16	0.31
10.025	0.00	0.00	10.950	9.96	0.27
10.050	0.01	0.00	10.975	9.65	0.34
10.075	0.03	0.00	11.000	9.60	0.37
10.100	0.05	0.00	11.025	9.58	0.54
10.125	0.08	0.00	11.050	9.66	0.52
10.150	0.14	0.00	11.075	10.71	0.47
10.175	0.34	0.00	11.100	10.39	0.54
10.200	1.10	0.00	11.125	10.07	0.48
10.225	3.46	0.00	11.150	10.13	0.66
10.250	4.44	0.00	11.175	10.74	0.80
10.275	4.57	0.00	11.200	10.76	0.73
10.300	5.00	0.00	11.225	10.78	0.87
10.325	5.14	0.00	11.250	11.35	0.85
10.350	6.04	0.00	11.275	11.40	1.00
10.375	6.20	0.00	11.300	11.69	0.96
10.400	7.34	0.00	11.325	11.28	1.04
10.425	7.54	0.00	11.350	11.66	0.83
10.450	7.49	0.00	11.375	12.15	1.14
10.475	7.72	0.00	11.400	11.43	1.18
10.500	8.25	0.00	11.425	12.02	1.19
10.525	8.13	0.00	11.450	12.13	1.27
10.550	7.92	0.00	11.475	12.91	1.37
10.575	8.59	0.00	11.500	12.33	1.29
10.600	9.02	0.00	11.525	12.90	1.52
10.625	8.75	0.00	11.550	13.53	1.54
10.650	9.13	0.00	11.575	13.20	1.67
10.675	9.06	0.00	11.600	13.51	1.78
10.700	8.64	0.00	11.625	12.57	1.96

10.725	9.14	0.00	11.650	12.90	1.99
10.750	8.82	0.00	11.675	13.63	1.95
10.775	9.04	0.04	11.700	12.95	2.24
10.800	9.13	0.03	11.275	12.63	1.40

Table S5. Absolute PI cross-sections (in Mb) for 2-methyl-1,3-dioxolane.

Energy (eV)	*m/z* 88	*m/z* 87	*m/z* 73	Energy (eV)	*m/z* 88	*m/z* 87	*m/z* 73
9.200	0.00	0.00	0.00	10.375	0.04	0.53	11.37
9.225	0.00	0.00	0.00	10.400	0.04	0.57	11.78
9.250	0.00	0.00	0.00	10.425	0.04	0.62	12.30
9.275	0.00	0.00	0.00	10.450	0.04	0.67	12.61
9.300	0.00	0.00	0.00	10.475	0.04	0.72	13.19
9.325	0.00	0.00	0.00	10.500	0.04	0.78	13.59
9.350	0.00	0.00	0.01	10.525	0.04	0.83	14.09
9.375	0.00	0.00	0.01	10.550	0.04	0.87	14.35
9.400	0.00	0.00	0.02	10.575	0.04	0.93	14.88
9.425	0.00	0.00	0.02	10.600	0.04	0.96	15.27
9.450	0.00	0.00	0.03	10.625	0.04	1.01	15.62
9.475	0.00	0.00	0.05	10.650	0.04	1.05	15.92
9.500	0.01	0.00	0.08	10.675	0.05	1.08	16.20
9.525	0.01	0.00	0.11	10.700	0.04	1.13	16.68
9.550	0.01	0.00	0.17	10.725	0.04	1.16	16.92
9.575	0.02	0.00	0.25	10.750	0.05	1.20	17.27
9.600	0.02	0.00	0.37	10.775	0.05	1.22	17.52
9.625	0.02	0.00	0.51	10.800	0.05	1.26	17.98
9.650	0.02	0.00	0.69	10.825	0.05	1.30	17.94
9.675	0.02	0.00	0.88	10.850	0.05	1.33	18.49
9.700	0.02	0.00	1.13	10.875	0.04	1.37	18.74
9.725	0.02	0.01	1.39	10.900	0.05	1.39	19.17
9.750	0.02	0.01	1.68	10.925	0.05	1.43	19.56
9.775	0.02	0.01	1.97	10.950	0.05	1.47	19.64
9.800	0.02	0.02	2.26	10.975	0.05	1.49	20.07
9.825	0.02	0.02	2.61	11.000	0.05	1.53	20.37
9.850	0.02	0.03	2.93	11.025	0.04	1.55	20.59
9.875	0.02	0.03	3.33	11.050	0.05	1.60	21.14
9.900	0.03	0.04	3.66	11.075	0.05	1.62	21.59
9.925	0.02	0.05	4.05	11.100	0.06	1.65	21.90
9.950	0.02	0.06	4.38	11.125	0.05	1.70	22.12
9.975	0.02	0.08	4.85	11.150	0.05	1.74	22.66
10.000	0.03	0.09	5.17	11.175	0.05	1.77	23.04
10.025	0.03	0.11	5.56	11.200	0.05	1.80	23.47
10.050	0.03	0.13	5.96	11.225	0.06	1.83	23.74
10.075	0.03	0.15	6.34	11.250	0.05	1.88	24.11
10.100	0.03	0.17	6.69	11.275	0.05	1.93	24.69
10.125	0.03	0.20	7.18	11.300	0.05	1.96	24.71
10.150	0.03	0.21	7.57	11.325	0.05	2.01	25.47
10.175	0.04	0.24	7.91	11.350	0.05	2.02	25.68
10.200	0.03	0.28	8.30	11.375	0.05	2.07	26.15
10.225	0.04	0.30	8.76	11.400	0.05	2.15	26.62
10.250	0.04	0.34	9.17	11.425	0.06	2.15	26.85
10.275	0.04	0.37	9.53	11.450	0.06	2.20	27.32
10.300	0.04	0.41	9.94	11.475	0.05	2.23	27.63
10.325	0.04	0.44	10.41	11.500	0.06	2.29	28.30
10.350	0.04	0.49	10.85	11.525	0.05	2.34	28.80

Quantification of stable reaction products from reference photoionization (PI) spectra.

A time-integrated (0-30 ms) background subtracted photoionization (PI) spectrum for diethyl ether (*m*/*z* 74) from Cl-initiated oxidation experiments at 7500 Torr, 450 K, and $[O_2] = 7\times10^{17}$ molecules/cm^3 is shown in Figure S6(top). The negative PI spectrum indicates the consumption of DEE from oxidation. Figure S6(bottom) provides the energy integrated (8.5 – 11 eV) time trace, in which the pre-photolysis signal has been scaled to match the initial DEE concentration (1×10^{14} molecules/cm^3).

Figure S7 shows the fits of the measured PI spectra (corrected for the MDF and photon flux) of six observed DEE oxidation products to the available reference spectra. These reaction products are quantified from equation (1), using the known DEE concentration as a reference. The resulting time-dependent absolute concentration profiles of these six DEE oxidation products are presented in Figure S8 and are discussed in the main text.

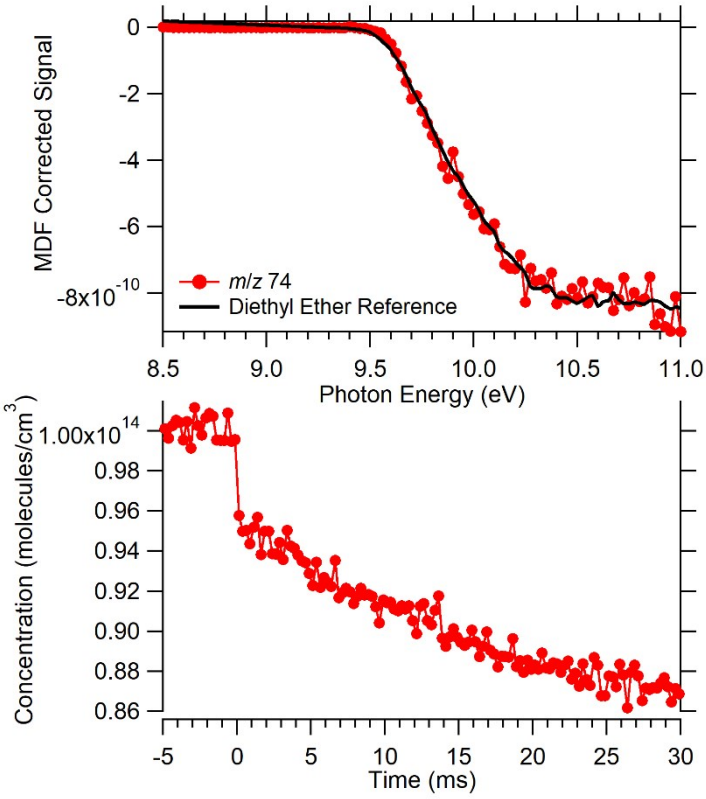

Figure S6. Top: Time-integrated (0-30 ms), background-subtracted PI spectrum for DEE (*m/z* = 74) at 7500 Torr, 450 K, and $[O_2] = 7\times10^{17}$ cm^{-3}. Bottom: Photon energy-integrated (8.5-11 eV) concentration-time profile for DEE showing the onset of DEE consumption at t = 0 ms initiated by the photolysis pulse.

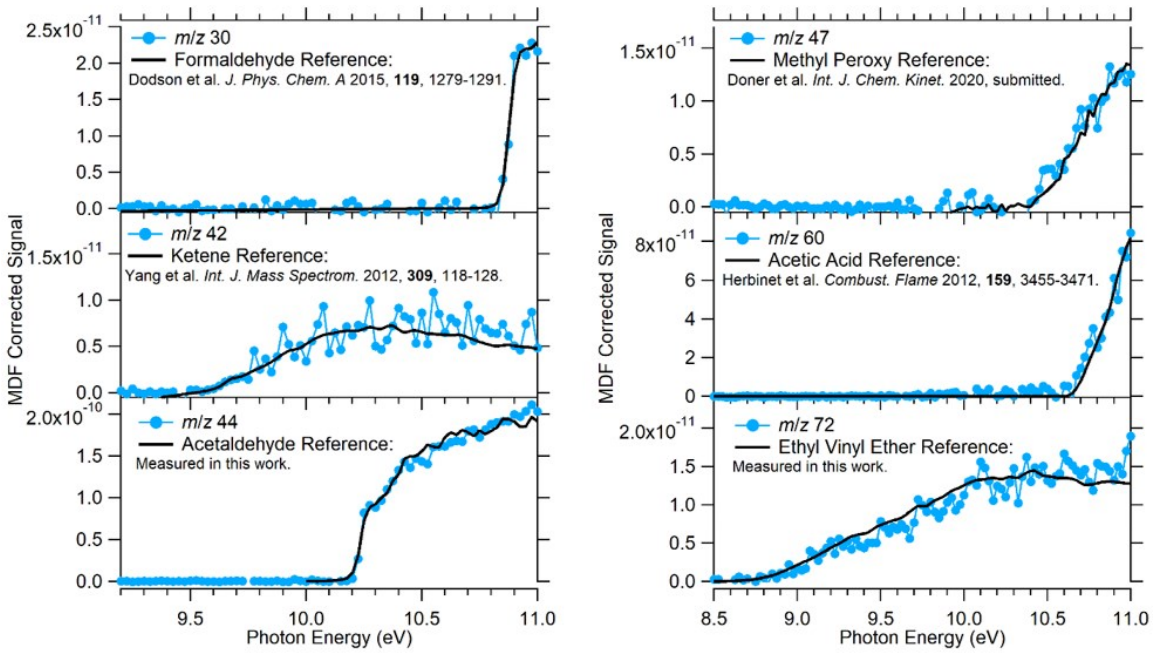

Figure S7. Time-integrated (0-30 ms) PI spectra (circles) for species identified from reference PI cross-section spectra (solid lines) in Cl-initiated diethyl ether (DEE) oxidation experiments at 7500 Torr, 450 K, and $[O_2] = 7\times10^{17}$ cm^{-3}. The reference PI cross-section spectra have been scaled to fit the experimentally measured spectra for quantification.

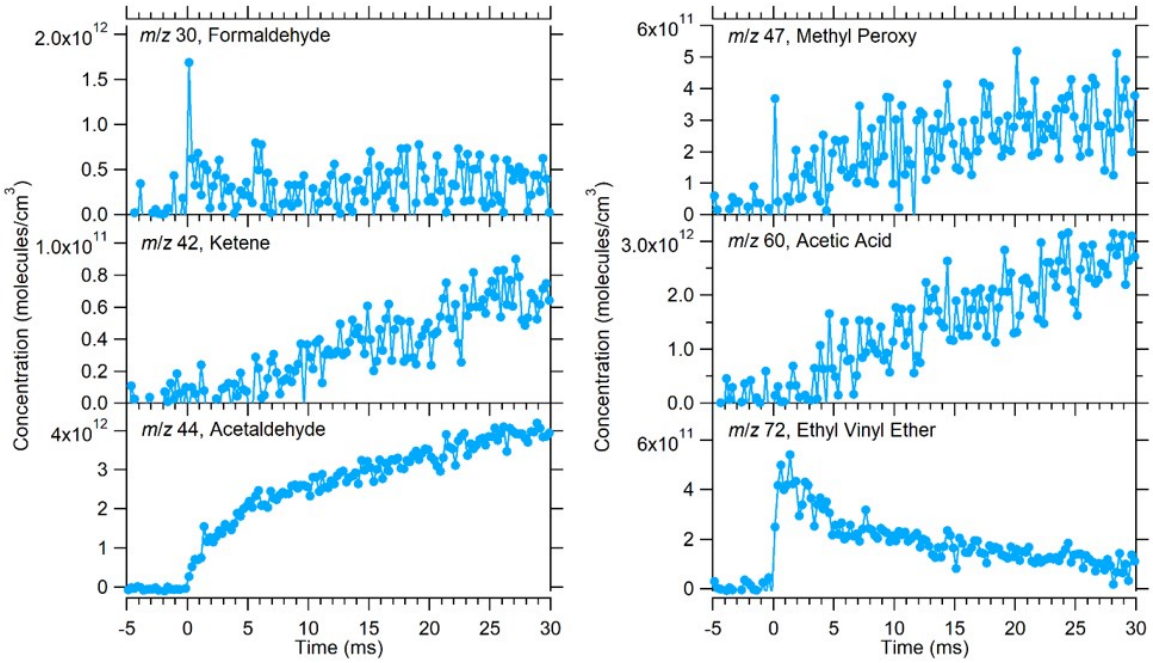

Figure S8. Absolute concentration profiles as a function of time for products identified from reference PI spectra at 7500 Torr, 450 K, and $[O_2] = 7\times10^{17}$ cm^{-3}. Concentrations were determined using equation (1) as described in the main text.

Calculations of cation potential energy surfaces (PESs).

To aid with assignments of dissociative ionization (DI) fragments of ROO•, •OOQOOH, and KHP, quantum chemical calculations were performed at the CBS-QB3 level of theory and the resulting PESs are shown in Figure S9. The PESs consider only the dominant isomers of ROO•, •OOQOOH, and KHP (one conformer for ROO• and •OOQOOH, and two conformers for KHP, which were chosen as a representative set to gauge the possible distribution of AIEs).

Calculations indicate that the ROO cation is unbound, with a calculated VIE of 9.98 eV to form ROO^+ in the triplet ground electronic state. After photoionization, ROO^+ undergoes barrierless O_2 elimination to form R^+ at *m/z* 73 with a calculated energy of 7.81 eV above that of neutral ROO• (Figure S9(a)). If the daughter ion R^+ is formed with enough internal energy, it can further fragment into CH_3CHOH^+ (*m/z* 45) + CH_2CH_2 via concerted 1,3-H transfer and C-O bond scission, with a calculated barrier of 9.22 eV. Based on the calculated PES, we expect to observe DI fragments at *m/z* 73 and 45 with appearance energies near the calculated VIE of ROO•, ~10 eV:

$CH_3CH_2OCH(OO)CH_3^+$	$\rightarrow CH_3CH_2OCHCH_3^+ + O_2$	*m/z* 73, AE ~10 eV
	$\rightarrow CH_3CHOH^+ + CH_2CH_2 + O_2$	*m/z* 45, AE ~10 eV

The OOQOOH cation is also unbound, with VIE = 10.07 eV. Upon photoionization, $OOQOOH^+$ eliminates neutral O_2 without a barrier to form $QOOH^+$ ($CH_3CH(OOH)OCHCH_3^+$) at *m/z* 105, with a calculated energy of 7.72 eV above •OOQOOH (Figure S9(b)). $QOOH^+$ may dissociate further without a barrier to CH_3CHOOH^+ (*m/z* 61) + CH_3CHO, with an asymptotic energy of 8.82 eV. There may be a concerted H transfer/C–O scission pathway to *m/z* 45 from the $QOOH^+$ fragment: $CH_3CH(OOH)OCHCH_3^+$ (*m/z* 105) → CH_3CHOH^+ (*m/z* 45) + CH_2CHOOH. The asymptotic energy of this channel is 9.34 eV. It is analogous to the *m/z* 45 forming channel from ROO^+; however, our calculations failed to optimize TSs leading to this channel, and we treat it as speculative. Lastly, we calculated asymptotic energies for the following channels:

$CH_3CH(OOH)OCH(OO)CH_3^+$	$\rightarrow CH_3CHOCH(OO)CH_3^+ + HO_2$	*m/z* 104, 9.91 eV
	$\rightarrow CH_3C(OOH)OCHCH_3^+ + HO_2$	*m/z* 104, 9.72 eV
	$\rightarrow CH_3CH(OOH)OCHCH_2^+ + HO_2$	*m/z* 104, 9.67 eV

The two latter channels require isomerization, whereas the first channel is direct via barrierless elimination of HO_2. We expect that the direct pathway is the most likely. In summary, we anticipate the following DI fragments from •OOQOOH, all with appearance energies near the VIE, ~10.1 eV:

$CH_3CH(OOH)OCH(OO)CH_3^+$	$\rightarrow CH_3CH(OOH)OCHCH_3^+ + O_2$	*m/z* 105, AE ~10.1 eV
	$\rightarrow CH_3CHOOH^+ + CH_3CHO + O_2$	*m/z* 61, AE ~10.1 eV
	$\rightarrow CH_3CHOH^+ + CH_2CHOOH + O_2$	*m/z* 45, AE ~10.1 eV
	$\rightarrow CH_3CHOCH(OO)CH_3^+ + HO_2$	*m/z* 104, AE ~10.1 eV

Both KHP conformers that we considered have bound cations with AIEs of 9.18 eV for the lowest-energy, H-bonded, conformer and 9.59 eV for the higher-energy conformer (Figure S9(c)). Both cation conformers can undergo barrierless decomposition to $CH_3C(O)OCHCH_3^+$ (*m/z* 87) + HO_2 with a calculated energy of 10.01 eV above the ground-state neutral conformer. The *m/z* 87 fragment ion can further decompose without a barrier to ultimately yield CH_3CO^+ (*m/z* 43) + $OCHCH_3$ + HO_2 with an energy of 11.07 eV. The KHP parent cation can also eliminate CH_3 via a barrier of 10.33 eV to yield a weakly-bound $CH_3CHOOH^+ \cdot CO_2$ adduct (*m/z* 105), which should rapidly lose CO_2 in a barrierless process to form CH_3CHOOH^+ (*m/z* 61) + CO_2 + CH_3 at an asymptotic energy of 10.15 eV. The asymptotic energies and barriers of the DI channels are higher than the AIE of KHP and thus correspond to the expected appearance energies of these fragment ions in our experiments. From the higher-energy KHP conformer, the appearance energies for all DI channels discussed above should be reduced by 0.19 eV.

$CH_3C(O)OCH(OOH)CH_3^+$	$\rightarrow CH_3C(O)OCH(OOH)CH_3^+$	*m/z* 120, AE ~9.2 eV
	$\rightarrow CH_3C(O)OCHCH_3^+ + HO_2$	*m/z* 87, AE ~10 eV
	$\rightarrow CH_3CO^+ + OCHCH_3 + HO_2$	*m/z* 43, AE ~11.1 eV
	$\rightarrow CH_3CHOOH^+ + CO_2 + CH_3$	*m/z* 61, AE ~10.3 eV

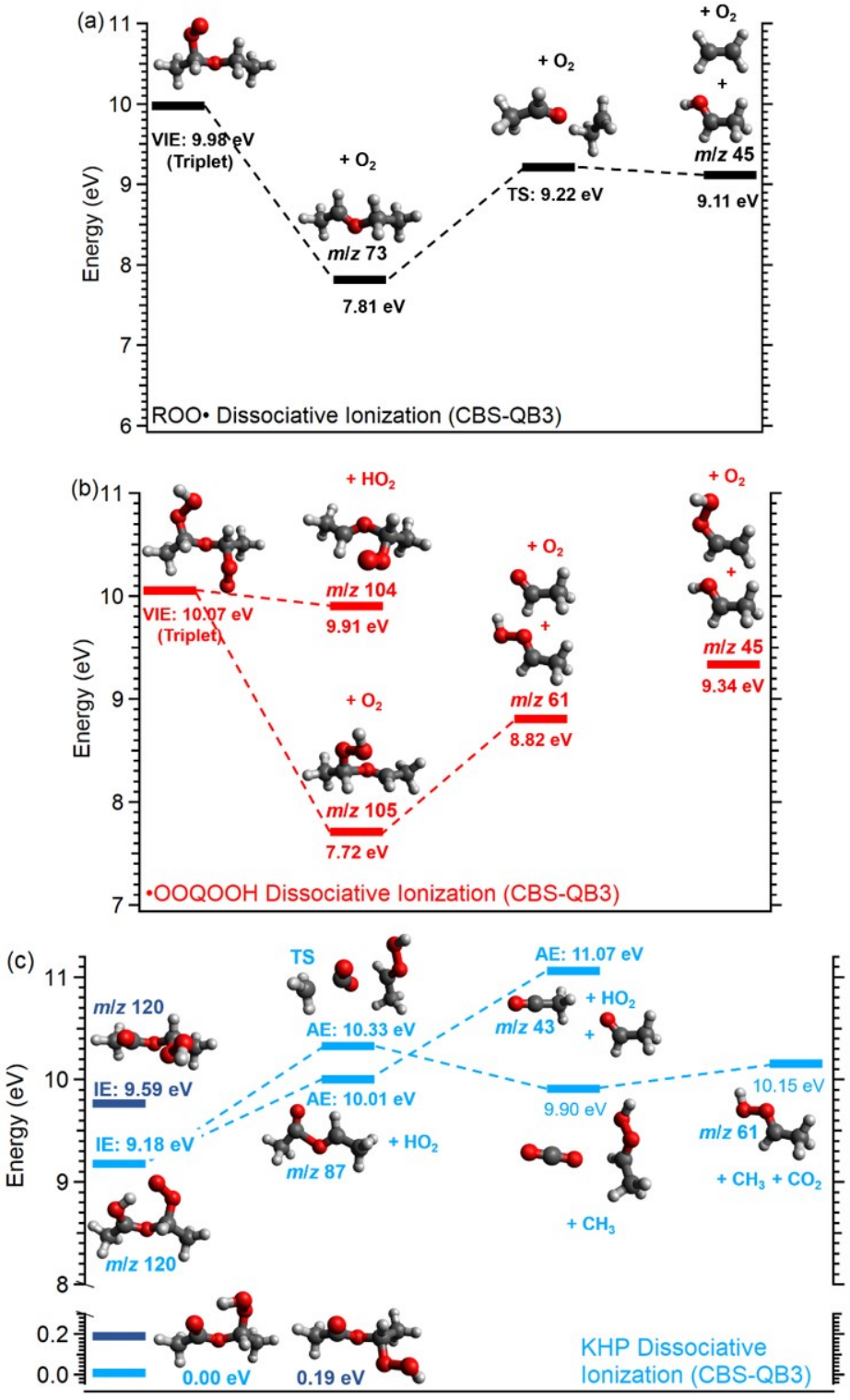

Figure S9. Cation potential energy surfaces, calculated with the CBS-QB3 method, for (a) ROO•, (b) •OOQOOH, and (c) KHP. State energies are referenced to the ground state of the neutral species. The detected fragment ion in each DI channel is labeled by its *m/z* value. For KHP in panel (c), the appearance energies for the daughter ions are given relative to the lowest energy neutral conformer. Appearance energies of daughter ions referenced to the higher energy KHP conformer are reduced by 0.19 eV.

Correcting the *m/z* 73 signal for the DI contribution of DEE.

According to the calculations, the major DI fragment of ROO• is R^+ (*m/z* 73), see Figure S9(a). However, DEE also produces a DI fragment at *m/z* 73. The contribution from the DEE DI fragment to the overall *m/z* 73 signal can be subtracted from the PI spectra and the kinetic time traces. A corrected PI spectrum for the DI fragment of ROO• is obtained as follows (see Figure S10(a)): 1) PI spectra of the *m/z* 74 parent ion and *m/z* 73 DI of DEE are integrated over -30 – 0 ms (prior to photolysis). The ratio of *m/z* 74:73 ion intensities is a molecular property of DEE and is constant, irrespective of kinetic time. 2) The post-photolysis depletion of the PI spectrum of the DEE parent ion is measured. The contribution of DEE DI to the *m/z* 73 PI spectrum is determined from the ratio of *m/z* 74:73 intensities, measured before photolysis. 3) The DEE DI contribution to *m/z* 73 is subtracted from the total *m/z* 73 PI spectrum. To correct for the DEE DI contribution to the *m/z* 73 time trace, the measured time trace of the parent ion of DEE (*m/z* 74) is scaled to match the pre-photolysis signal at *m/z* 73 and is subsequently subtracted, as shown in Figure S10(b).

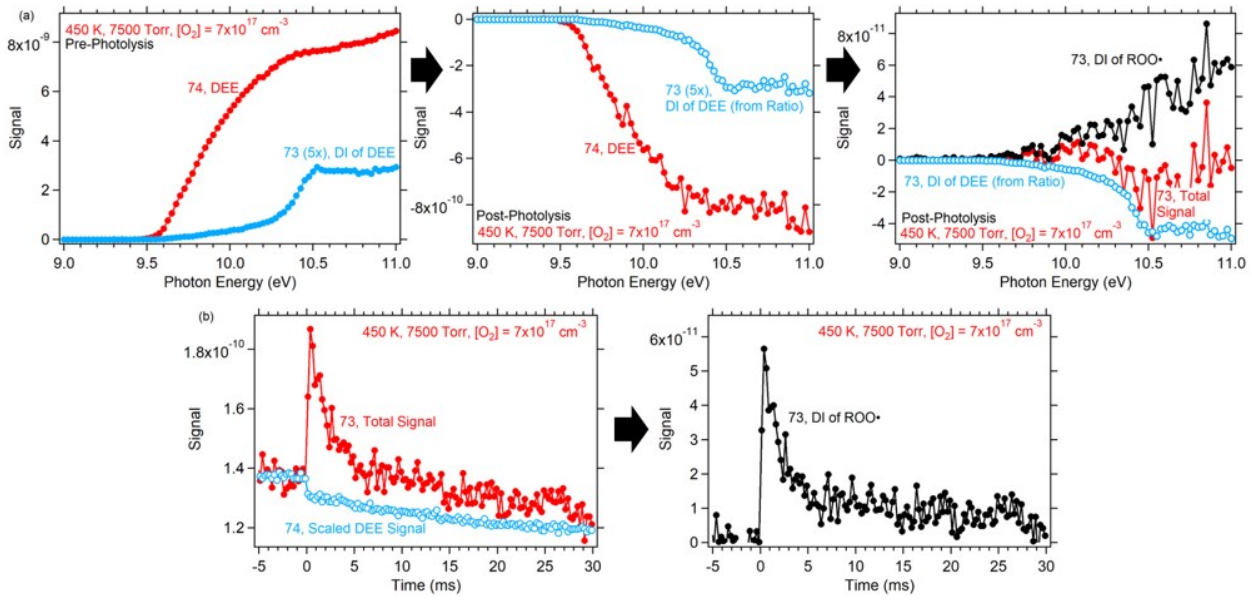

Figure S10. (a) Procedure for obtaining the PI spectrum of the ROO• DI fragment at *m/z* 73. (b) Procedure for correcting the time dependent signal measured at *m/z* 73 for the contribution of the DEE DI fragment to yield the signal solely arising from the DI fragment of ROO•. For details, see text.

Analysis of DI peaks (other than *m/z* 61) with multiple contributions.

m/z 45. The stable species already identified from reference PI spectra are known to produce no daughter ions at *m*/*z* 45 in the photon energy range measured. On the other hand, as described above, our calculations suggest that DI into the *m/z* 45 channel is possible for ROO• and •OOQOOH. The time-integrated (0-30 ms) PI spectrum for *m*/*z* 45, shown in Figure S11(a), has an ionization onset near 9.9 eV, which is consistent with the calculated VIEs for ROO• and •OOQOOH. Furthermore, the time-dependent signal for *m*/*z* 45 can be reproduced well using a weighted sum of ROO• and •OOQOOH time traces, with negligible contribution for the KHP time trace (Figure S11(b)), suggesting that *m*/*z* 45 ions are likely produced by the DI of only ROO• and •OOQOOH. Because our calculations of the possible sources of *m/z* 45 ions are not conclusive, we do not attempt to deconvolve its PI spectrum or extract absolute PI cross-sections.

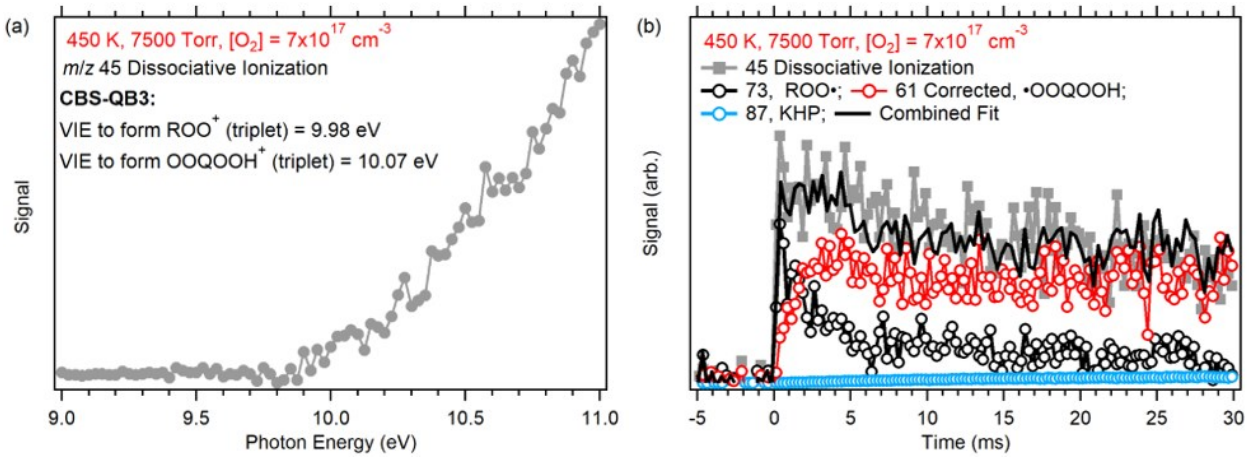

Figure S11. (a) Time-integrated (0-30 ms) PI spectrum for the *m/z* 45 peak at 450 K and 7500 Torr. The energy-integrated (8.5-11 eV) time trace of *m/z* 45 ions (gray) is shown in (b), along with the fit to a weighted sum of ROO•, •OOQOOH, and KHP.

m/z 43. The PI spectrum for the *m*/*z* 43 peak has an onset near 10.2 eV as shown in Figure S12(a). We can rule out that the *m*/*z* 43 ions correspond to direct ionization of the acetyl radical on the basis of the AIE (~7 eV)[5] of acetyl. Different time behavior can be obtained for the *m*/*z* 43 ion if integration is performed

over photon energies of 8.5 – 10.6 eV and 8.5 – 11 eV, indicating the presence of at least two DI contributions, as demonstrated in Figure S12(b). The slow rise of the higher-energy portion of the *m/z* 43 signal is consistent with KHP time evolution. Our calculations identified a possible *m*/*z* 43 DI fragment from KHP, with an asymptotic energy of 10.88 or 11.07 eV, depending on which KHP conformer is ionized. The time trace for *m*/*z* 43 can be reproduced well by a weighted sum of time traces for ROO•, •OOQOOH, and KHP (Figure S12(c)), suggesting that *m*/*z* 43 DI fragments may arise from all three intermediates. In addition, other contributions may exist. Four of the observed species in Table 1 in the main text do not contribute to the *m/z* 43 signal: formaldehyde and ketene are too small; methyl peroxy and acetic acid are known to have no *m/z* 43 daughter ions in our energy range. Two species from Table 1 contribute small DI signals at *m/z* 43: ethyl vinyl ether is a minor product (see Figure S8); acetaldehyde is a major product but its PI cross-section into the *m/z* 43 DI channel is small. The KHP decomposition product acetic anhydride forms a DI fragment at *m*/*z* 43 with an onset near 10.4 eV (see Figure S4). We estimate that the PI cross-section of acetic anhydride into the parent cation channel at *m*/*z* 102 is ~0.08 Mb at these conditions. In our DEE oxidation experiments at 450 K and 7500 Torr, we find essentially no ion signal at *m/z* 102. Based on the noise level, we estimate an upper limit of $\sim 2 \times 10^{11}$ molecules/cm^3 for the average concentration of acetic anhydride. Thus, if present, acetic anhydride is not a major product (at most, average mole fraction of ~0.02). In summary, the *m/z* 43 peak comes from as many as six DI contributions, but does not include any substantial sources that are not already listed in Table 1 and that would impact our quantification strategy described in the main text.

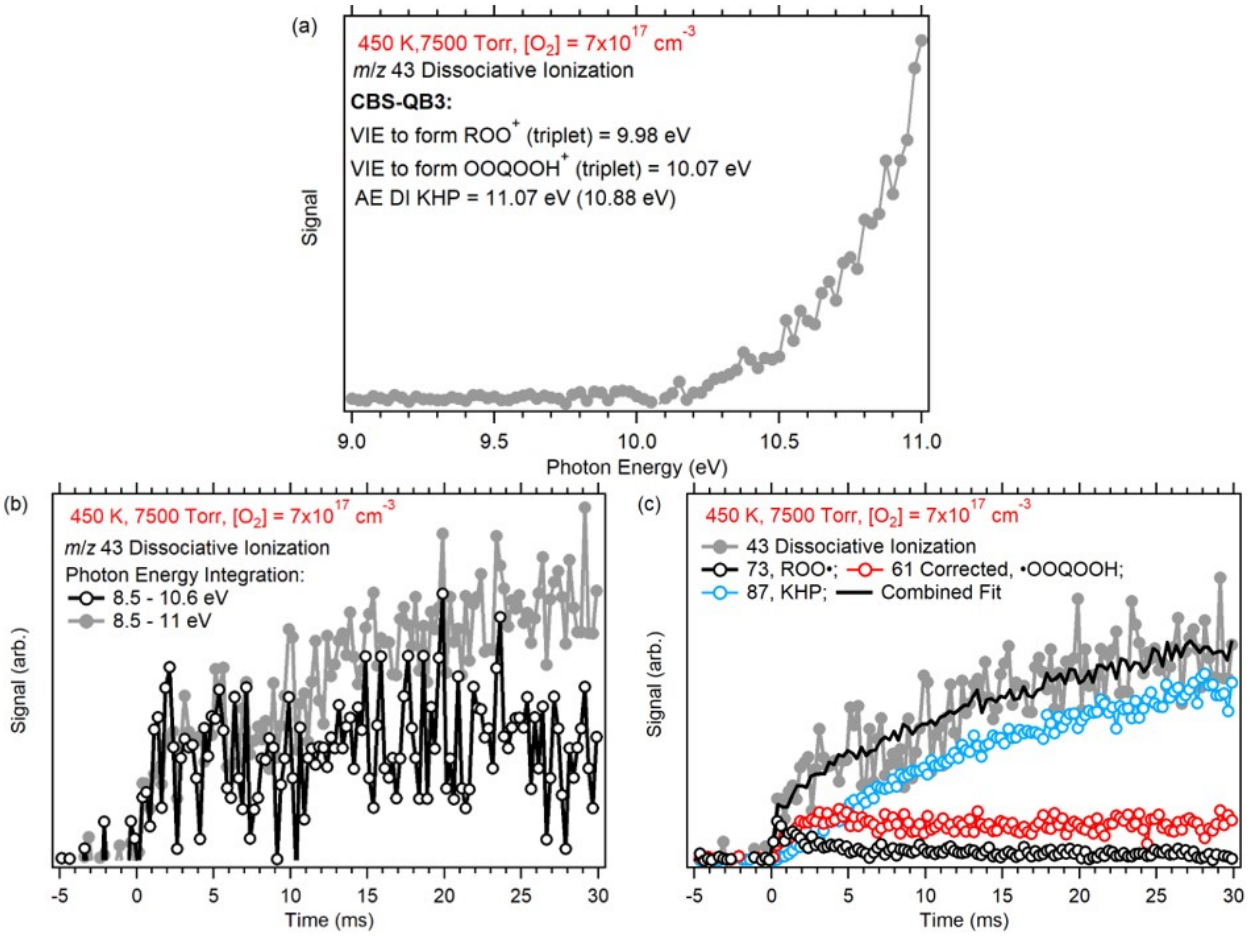

Figure S12. (a) Time-integrated (0-30 ms) PI spectrum for the *m/z* 43 peak at 450 K and 7500 Torr. (b) Time-dependent signal for *m/z* 43, integrated over photon energies 8.5 – 10.6 eV (black) and 8.5 – 11.0 eV (gray). (c) Energy-integrated (8.5-11.0 eV) time dependent signal for *m/z* 43 (gray), along with a fit (line) to a weighted sum of ROO• (black), •OOQOOH (red), and KHP (blue) time signals.

m/z 104. The PI spectrum for *m*/*z* 104 is shown in Figure S13(a) and has an onset near 10 eV. This is consistent with our calculations of possible DI fragments into the *m/z* 104 channel from •OOQOOH. A comparison of the time traces for *m*/*z* 104 and 105, shown in Figure S13(b), indicates that they are nearly identical, in support of the signal at *m*/*z* 104 arising from DI of •OOQOOH. Another possibility for *m/z* 104 ions is direct ionization of a distinct DEE oxidation product (hydroperoxyethyl vinyl ether), which may form via HO_2 elimination from neutral •OOQOOH ($CH_3CH(OOH)OCH(OO)CH_3$ → $CH_3CH(OOH)OCH{=}CH_2 + HO_2$), in analogy to our study of THF.[6] However, the calculated AIE for this

product is 8.6 eV and no signal is evident in the PI spectrum below ~10 eV, suggesting that it is not a major reaction channel in DEE oxidation.

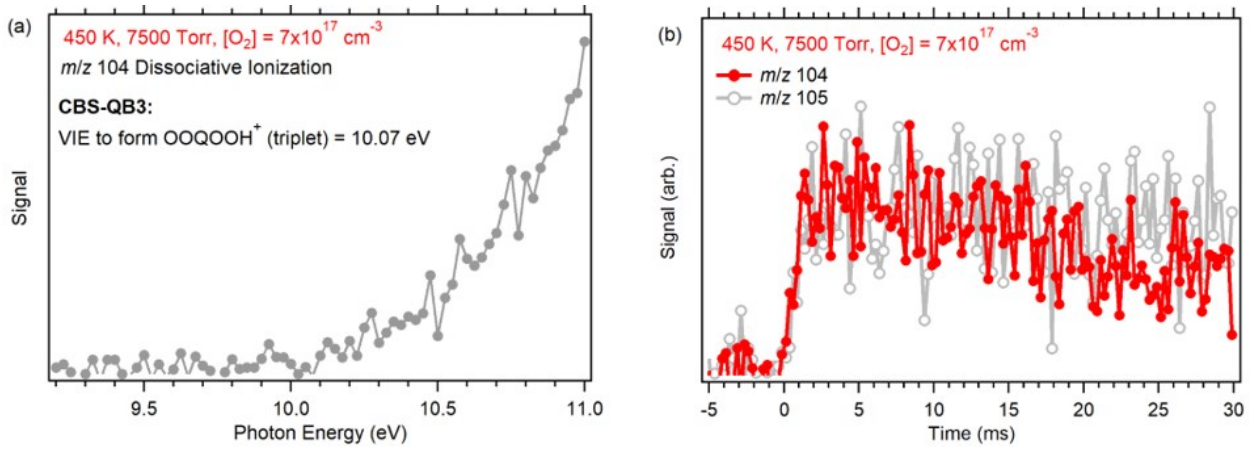

Figure S13. (a) Time-integrated (0-30 ms) PI spectrum for *m/z* 104 measured in DEE oxidation experiments at 450 K and 7500 Torr. (b) Comparison between the energy-integrated (8.5 – 11 eV) time traces for *m/z* 104 (closed circles) and 105 (open circles) at the same conditions.

Quantification of ROO•, •OOQOOH, and KHP at 400 K.

Figure S14 shows the analysis of the kinetics of ROO•, •OOQOOH, and KHP at T = 400 K and P = 7300 Torr. At this temperature, intermediates are better separated in time than at 450 K. However, the relative abundances of ROO•, •OOQOOH, and KHP change with temperature, such that at 400 K the concentration of ROO• is significantly higher than those of •OOQOOH and KHP, compared with the results at 450 K, where all three intermediates have similar abundances. The deconvolution method that was used at 450 K to successfully quantify ROO•, •OOQOOH, and KHP from carbon atom balance fails at 400 K. It produces fit coefficients for the •OOQOOH and KHP concentrations that are strongly correlated and have large uncertainties because of their small contributions and the noisy data (Figure S14(b)). Nonetheless, the concentration of ROO• can still be determined reliably at 400 K because it is solely responsible for the missing C atom balance at kinetic times immediately after t = 0 ms. The ROO• concentration is obtained by scaling the time signal of the *m/z* 73 DI fragment to reproduce the missing concentration at t = ~0 ms.

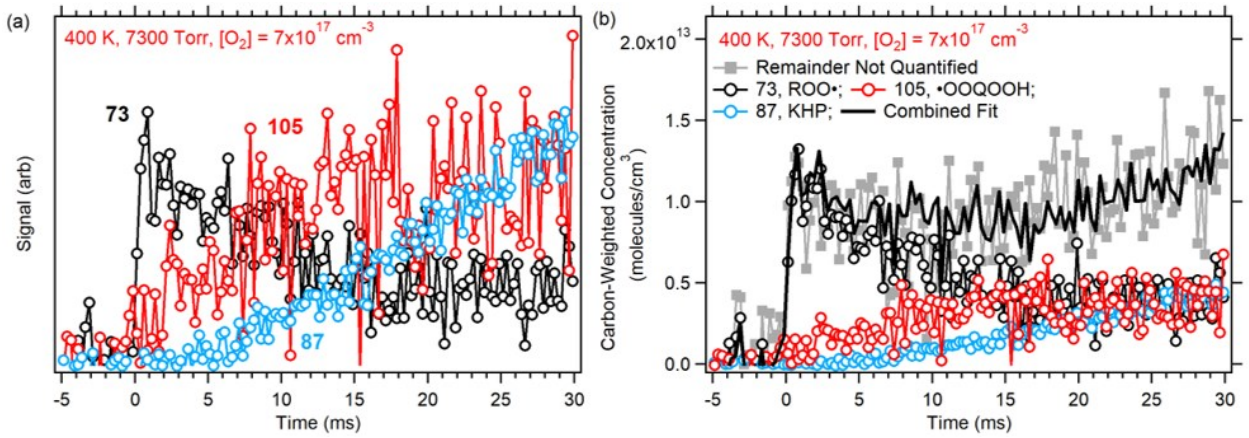

Figure S14. (a) Time traces (scaled for visual comparison) for ions at *m*/*z* 73, 105, and 87 in oxidation experiments of DEE at 400 K and 7300 Torr integrated over 8.7-11 eV. The *m*/z 73 ion signal was corrected for the DI contribution of DEE. (b) Time dependent carbon-weighted total concentration of unquantified products (gray squares), i.e. the difference between the carbon-weighted DEE consumption and the sum of quantified products. The solid black line results from a weighted sum of the time traces for ROO• (*m*/*z* 73, black circles), •OOQOOH (*m*/*z* 105, red circles), and KHP (*m*/*z* 87, blue circles).

The absolute PI cross-section of ROO•.

We obtained the PI cross-section of ROO• into its *m*/*z* 73 DI fragment from multiple experiments. One measurement was performed at 450 K, 50 Torr, and $[O_2]$ = ~2.5×10^{17} cm^{-3} using an established low-pressure MPIMS instrument;[1] the other 5 measurements were done on the high-pressure MPIMS instrument. The PI cross-sections from all measurements are plotted in Figure S15 and agree well with each other. The differences in the measurements are due to systematic errors in the mass-dependent bias correction and in the DEE DI fragment correction and due to statistical noise in the data. The final reported PI cross-section of the ROO• DI fragment in the main text is the average of these six measurements with error bars corresponding to one standard deviation.

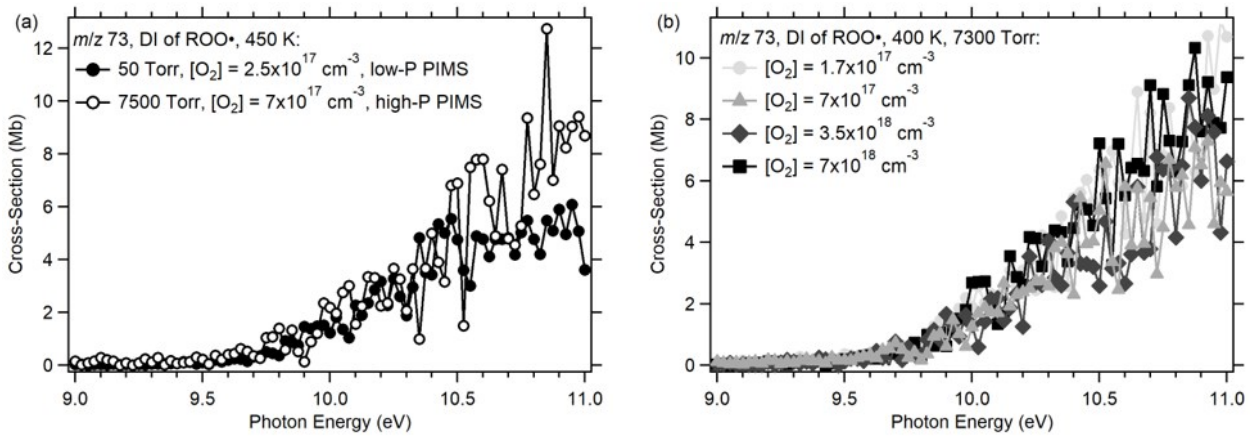

Figure S15. Comparison of the absolute PI cross-sections for the *m/z* 73 DI channel of ROO•, determined from six independent measurements: (a) 7500 Torr, 450 K, $[O_2] = 7\times10^{17}$ cm^{-3}, and 50 Torr, 450 K, $[O_2] = 2.5\times10^{17}$ cm^{-3}; (b) 400 K, 7300 Torr, $[O_2] = (1.7 – 70) \times10^{17}$ cm^{-3}.

The parent ion PI cross-section of KHP.

The PI cross-section of KHP into the weak parent ion peak at *m/z* 120 was obtained relative that of the intense *m/z* 61 DI peak, using experiments with very high $[O_2]$, $[Cl]_{t=0}$, and [DEE] to maximize the KHP production. Figure S16 shows the PI spectra and time traces of the *m/z* 61 and 120 ions measured in "high-concentration" experiments at 7300 Torr and 500 K. The *m/z* 61 PI spectrum from the baseline experiments is also included in Figure S16(a) (red solid line). We do not include the *m/z* 87 spectrum because it contains contributions from a new species, 2-methyl-1,3-dioxolane, which we observe at the "high-concentration" conditions. The presence of 2-methyl 1,3-dioxolane is confirmed by its parent ion signal at *m/z* 88, and it also has a strong DI peak at *m/z* 87 (see Figure S5). In contrast, the *m*/*z* 61 PI spectra from our baseline and high O_2, Cl, and DEE experiments agree relatively well with each other, suggesting that no new contributions are present at *m/z* 61. Thus, the PI cross-section for the *m*/*z* 120 KHP parent cation can be determined by referencing to the cross-section of the *m*/*z* 61 DI fragment, determined at our baseline condition. The resulting cross-section for the KHP parent cation (*m*/*z* 120) is shown in Figure 8(c) of the main text.

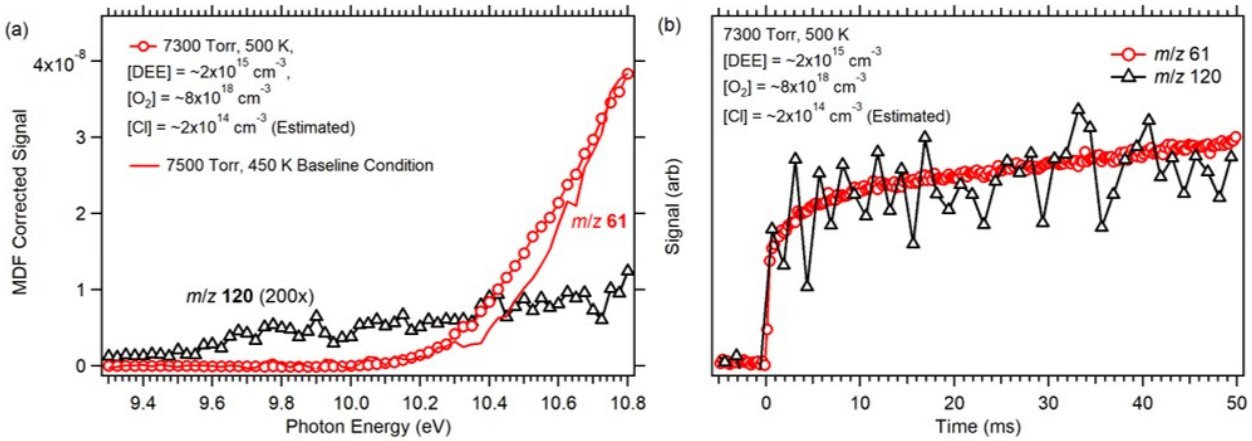

Figure S16. (a) PI spectra (integrated over 0-50 ms) of the KHP ions collected at "high concentration" conditions (500 K, 7300 Torr, symbols) and at the baseline conditions (450 K, 7500 Torr, line). The "baseline" PI spectrum is scaled for visual comparison. (b) Time-dependent signals (integrated over 9.0-10.8 eV) for *m*/*z* 120 and 61 ions at the high $[O_2]$, [Cl], and [DEE] conditions.

Dependence of PI cross-sections on sampling expansion.

Figure S17 shows the PI spectra (symbols) of the KHP DI fragments at *m*/*z* 87 and 61 (corrected for the •OOQOOH contribution), acquired at 500 K and P = 1500, 3750, and 7500 Torr. The *m*/*z* 87 KHP spectra are overlaid with the spectra from P = 7500 Torr and T = 450 K, which are shifted to lower photon energies by 0.08 and 0.15 eV in the measurements at 3750 and 1500 Torr, respectively. In contrast, the PI spectra of all other species exhibit no pressure dependent shifts. In addition, there is no evidence here for new products, such as 2-methyl-1,3-dioxolane, that could explain the shift to lower onsets at *m*/*z* 87 (as was the case for the high O_2, Cl, and DEE condition discussed above). Our conclusion, therefore, is that KHP exhibits energy shifts in its PI spectrum due to changing gas pressures affecting the sampling expansion.

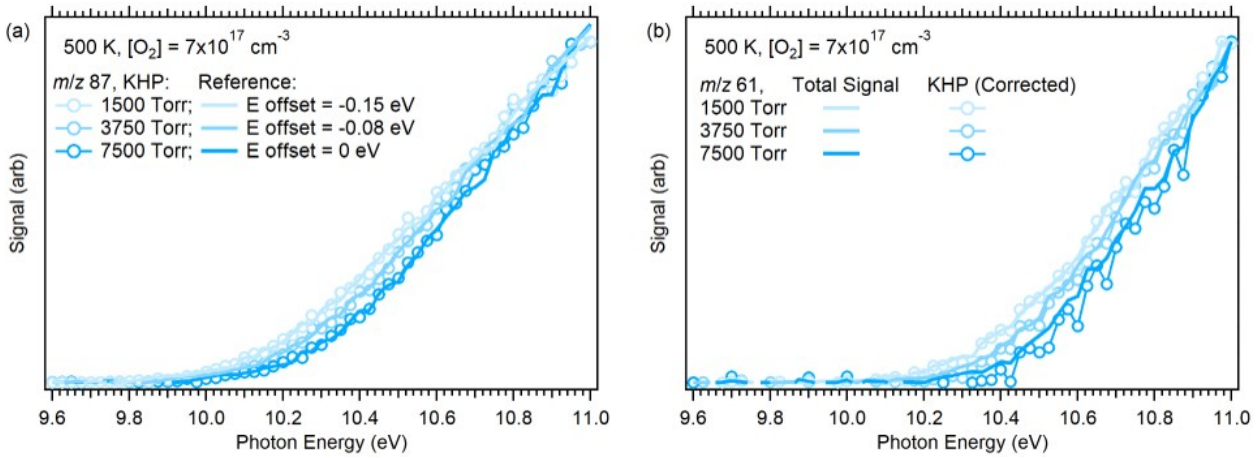

Figure S17. PI spectra (integrated over 0-30 ms) at P = 1500 – 7500 Torr and T = 500 K of the KHP DI fragments at (a) *m*/*z* 87 and (b) *m*/*z* 61 (corrected for the •OOQOOH contribution). The spectra are scaled for comparison and superimposed with the PI spectra (solid lines) from 450 K and 7500 Torr, which were shifted by -0.15 eV (at 1500 Torr) and -0.08 eV (at 3750 Torr).

Quantification at other experimental conditions.

Absolute PI cross-sections of ROO• (*m*/*z* 73), •OOQOOH (*m*/*z* 105), and KHP (*m*/*z* 87), determined at T = 450 K and P = 7500 Torr, were used as references to quantify these intermediates at other conditions, as summarized in Table S1. Concentration-time profiles of ROO•, •OOQOOH, and KHP, obtained using equation (1), are shown in Figures S18 – S20 as a function of temperature, pressure, and O_2 concentration. These figures also show the overall carbon atom balance, calculated as the ratio of the sum of all quantified products (now explicitly including ROO•, •OOQOOH, and KHP) to DEE consumption.

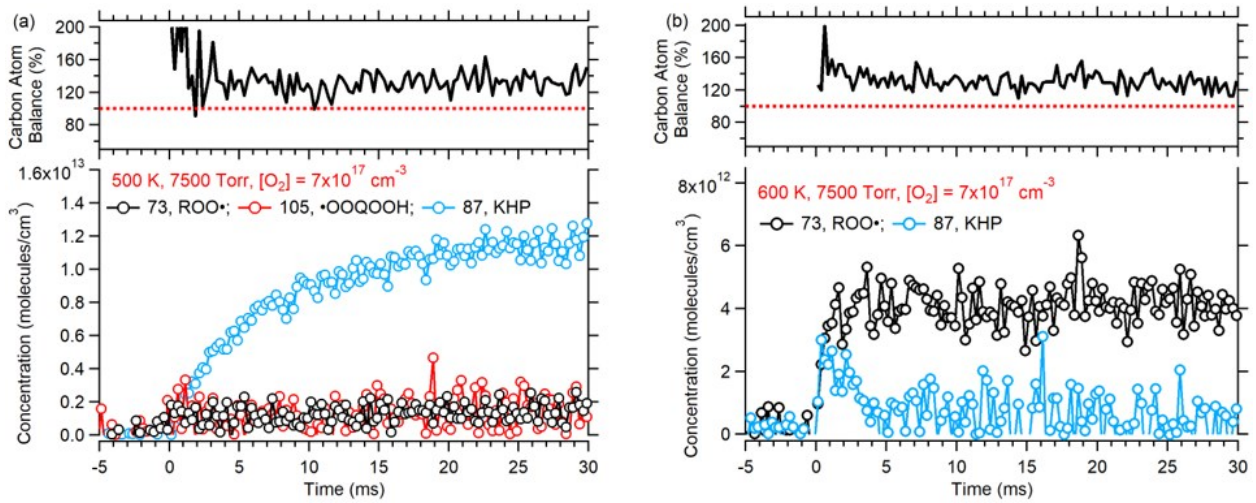

Figure S18. Concentration-time profiles for ROO• (black circles), •OOQOOH (red circles), and KHP (blue circles), along with the carbon atom balance at 7500 Torr, $[O_2] = 7\times10^{17}$ cm^{-3}, and (a) 500 K, or (b) 600 K.

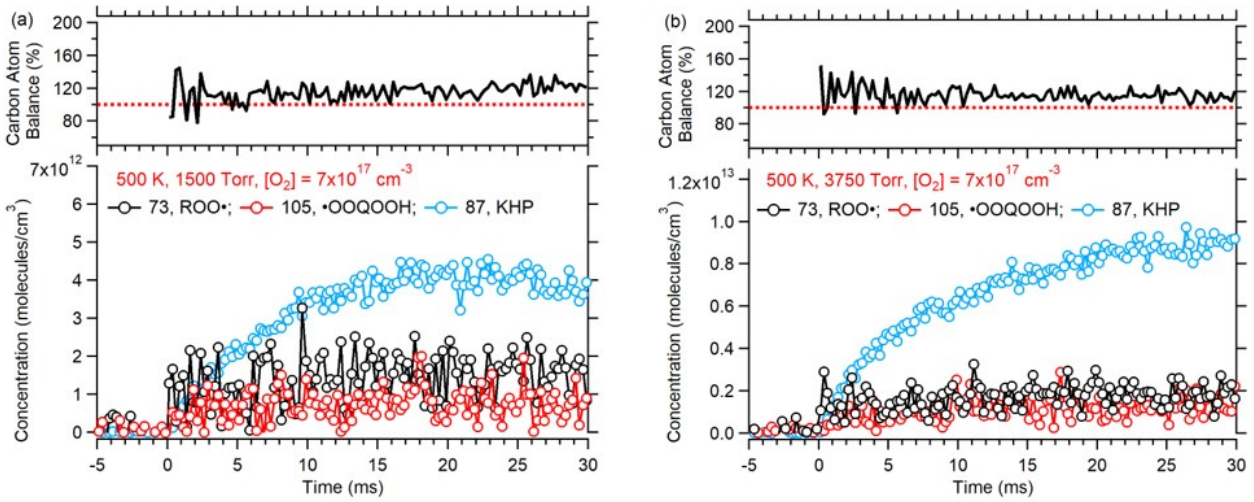

Figure S19. Concentration-time profiles for ROO• (black circles), •OOQOOH (red circles), and KHP (blue circles), along with the carbon atom balance at 500 K, $[O_2] = 7\times10^{17}$ and (a) 1500 Torr, or (b) 3750 Torr.

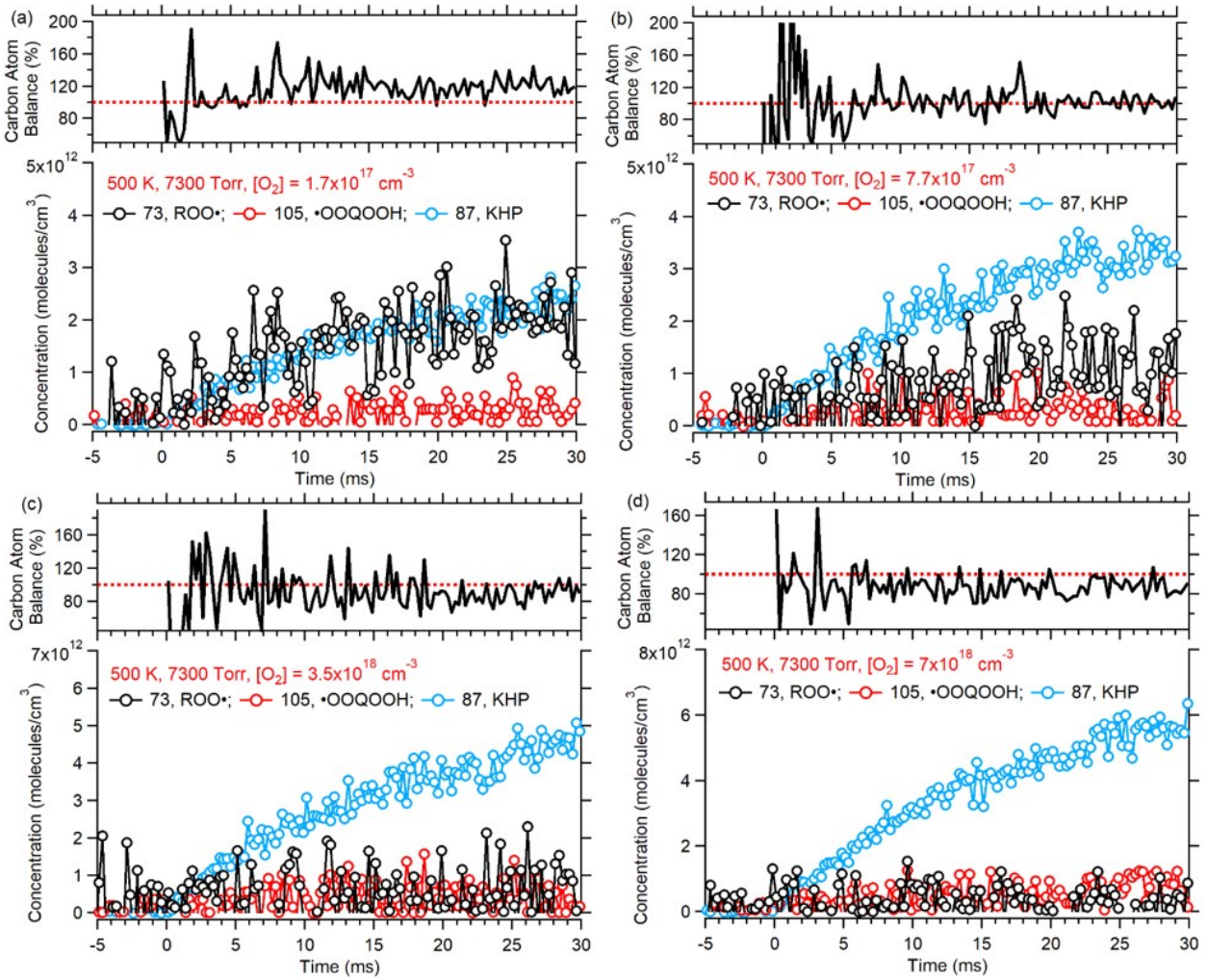

Figure S20. Concentration-time profiles for ROO• (black circles), •OOQOOH (red circles), and KHP (blue circles), along with the carbon atom balance at 7300 Torr, 500 K, and $[O_2]$ of (a) 1.7×10^{17}, (b) 7×10^{17}, (c) 3.5×10^{18}, or (d) 7×10^{18} cm^{-3}.

Effects of pressure-dependent KHP PI cross-sections on quantification.

Figure S21 shows the upper and lower-bound estimates of the KHP PI cross-sections for the measurements at 1500 and 3750 Torr. Figure S21(a) shows the reference *m/z* 87 PI cross-section from Figure 8, either simply shifted by -0.15 eV (open circles) or both shifted and scaled to maintain the same area under the PI spectrum (closed circles) for P = 1500 Torr. Figure S21(b) shows the same treatment for P = 3750 Torr, except that the shift is -0.08 eV. Figures S21(c) and (d) demonstrate the resulting lower- and upper-bound KHP concentration-time profiles and deviations in the overall C atom balance. The carbon imbalance is ~17% (~27%) at both pressures when lower- (upper)-bound KHP concentration is used.

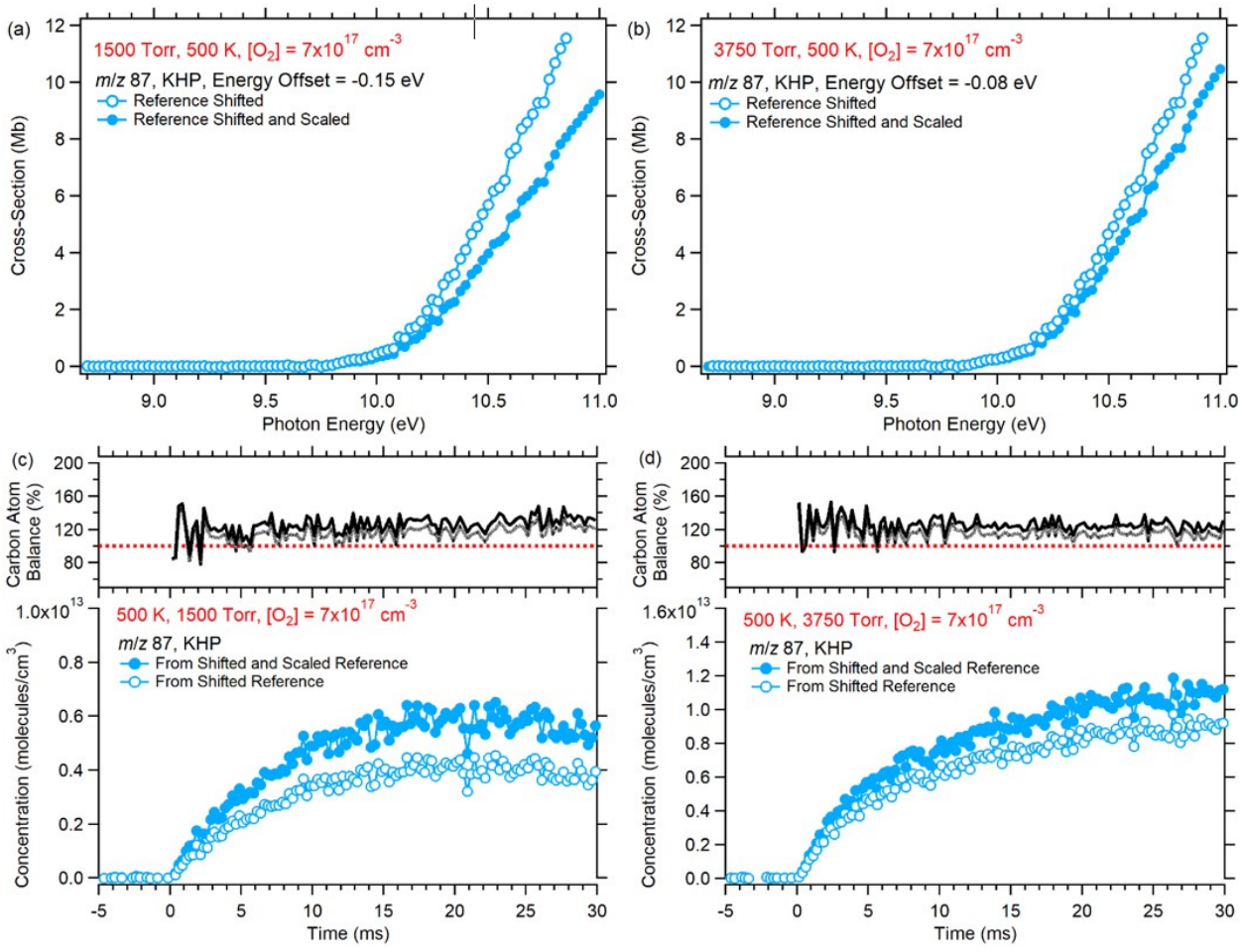

Figure S21. Estimated upper- and lower-bound PI cross-sections for the *m/z* 87 DI fragment of KHP at (a) 1500 Torr and (b) 3750 Torr. Resulting lower- and upper-bound KHP concentration-time profiles are shown in (c) for 1500 Torr and (d) for 3750 Torr, with corresponding carbon atom balances.

References

1. D. L. Osborn, P. Zou, H. Johnsen, C. C. Hayden, C. A. Taatjes, V. D. Knyazev, S. W. North, D. S. Peterka, M. Ahmed and S. R. Leone, *Rev. Sci. Instrum.*, 2008, **79**, 104103.
2. J. C. Person and P. P. Nicole, *J. Chem. Phys.*, 1970, **53**, 1767-1774.
3. T. A. Cool, J. Wang, K. Nakajima, C. A. Taatjes and A. McLlroy, *Int. J. Mass spectrom.*, 2005, **247**, 18-27.
4. T. A. Cool, K. Nakajima, T. A. Mostefaoui, F. Qi, A. McIlroy, P. R. Westmoreland, M. E. Law, L. Poisson, D. S. Peterka and M. Ahmed, *J. Chem. Phys.*, 2003, **119**, 8356-8365.
5. S. G. Lias, J. E. Bartmess, J. F. Liebman, J. L. Holmes, R. D. Levin and W. G. Mallard, *J. Phys. Chem. Ref. Data, Suppl. 1*, 1988, **17**, 1-861.
6. I. O. Antonov, J. Zador, B. Rotavera, E. Papajak, D. L. Osborn, C. A. Taatjes and L. Sheps, *J. Phys. Chem. A*, 2016, **120**, 6582-6595.